Substrate-Induced Fano Resonances of a Plasmonic: Nanocube: A Route to Increased-Sensitivity Localized Surface Plasmon Resonance Sensors Revealed

ARTICLE *in* NANO LETTERS · MARCH 2011

Impact Factor: 13.59 · DOI: 10.1021/nl200135r · Source: PubMed

NANO LETTERS

LETTER

pubs.acs.org/NanoLett

Substrate-Induced Fano Resonances of a Plasmonic Nanocube: A Route to Increased-Sensitivity Localized Surface Plasmon Resonance Sensors Revealed

Shunping Zhang,[†] Kui Bao,[‡] Naomi J. Halas,[†,‡] Hongxing Xu,[†] and Peter Nordlander*[,†,‡]

[†]Beijing National Laboratory for Condensed Matter Physics, and Institute of Physics, Chinese Academy of Sciences, Box 603-146, 100190, Beijing, China

[‡]Laboratory for Nanophotonics, Department of Physics and Electrical and Computer Engineering, Rice University, Houston Texas 77005, United States

ABSTRACT: Symmetry-breaking introduced by an adjacent semi-infinite dielectric can introduce coupling and hybridization of the plasmon modes of a metallic nanostructure. This effect is particularly large for entities with a large contact area adjacent to the dielectric. For a nanocube, a nearby dielectric mediates an interaction between bright dipolar and dark quadrupolar modes, resulting in bonding and antibonding hybridized modes. The Fano resonance that dominates the scattering spectrum arises from the interference of these modes. This analysis provides a strategy for optimizing the sensitivity of nanostructures, whether chemically synthesized or grown by deposition methods, as high-performance localized surface plasmon resonance sensors.

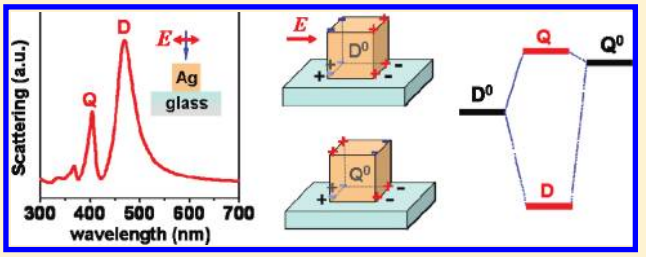

KEYWORDS: Plasmonics, Fano resonance, nanocube, substrate, LSPR sensing

Surface plasmons, defined as collective oscillations of the delocalized electrons in metallic nanostructures, are currently of tremendous interest for a broad range of emerging applications,[1] from chemical and biomolecular sensing[2−5] to energy harvesting[6] to subwavelength optical imaging[7−13] to waveguiding.[14,15] For complex nanostructures consisting of multiple closely spaced nanoparticles or patterned nanostructures, the plasmon modes of the individual nanoparticle can interact and form hybridized bonding and antibonding plasmon modes.[16−21] The collective modes of these systems can also be classified as "bright" or "dark" modes. Bright plasmon modes possess finite dipole moments and can therefore be efficiently excited by incident light. Since the bright modes couple to light, they also radiate, and their spectral features can be significantly broadened due to radiative damping. In contrast, dark plasmon modes possess zero dipole moments, do not couple efficiently to light, and are therefore not radiatively broadened. The dominant damping mechanism for dark modes is their intrinsic broadening, due to the imaginary part of the dielectric function of the metal: therefore the dark plasmon modes can be significantly narrower than the bright plasmon modes. Since most experimentally realizable plasmonic nanostructures are somewhat larger than the quasi-static, or dipole limit, most of their plasmon modes contain some admixture of dipole moments. For these systems the classification of a mode being dark or bright will thus depend on whether its dipole moment is small or large, with bright modes being those clearly visible in the optical spectrum.

Recently, much research has been focused on plasmonic structures that exhibit Fano resonances in their optical spectra.[22−26] Fano resonances arise directly from the coherent coupling and interference of bright and dark plasmon modes. Due to their microscopic origin as an interference phenomenon, plasmonic Fano resonances have been shown to be significantly more sensitive to the local dielectric environment than the primitive plasmon modes of the nanostructure, greatly enhancing the sensitivity of localized surface plasmon resonance (LSPR) sensors.[27−29] Since the line shapes of Fano resonances are determined by the width of the narrow, dark plasmon mode, sensors based on this effect have shown large increases in the LSPR figure of merit (FoM).[30]

The fundamental requirement for a Fano resonance is a weak coupling and interference between a dark and bright plasmon mode. This coupling can be controlled by symmetry breaking.[31,32] In planar ring−disk geometries or three-dimensional metallic sphere−shell structures, displacing the center particle with respect to the center of the surrounding ring or shell can introduce a coupling between the dark quadrupolar and bright dipolar modes of the structure.[27,33,34] In adjacent nanoparticle pairs, changing the size or composition of one of the nanoparticles can introduce a coupling between its collective dark and bright dimer modes.[35−38] Another type of symmetry breaking that can introduce a coupling between dark and bright modes is the introduction of an anisotropic environment, such as depositing a nanoparticle, or fabricating a nanostructure by deposition methods, onto a

Received: January 13, 2011
Revised: February 28, 2011
Published: March 16, 2011

dielectric substrate.[39−41] For a spherical nanoparticle in vacuum, there is no coupling between the bright dipolar and dark quadrupolar modes. However, when the nanoparticle is placed on a dielectric substrate, the "image" of a dipolar plasmon will have a significant quadrupolar field component across the nanoparticle, introducing a coupling between its dipolar and quadrupolar plasmons. The resulting hybridized plasmon modes will therefore be superpositions of both dipolar and quadrupolar modes. For example, for nanoshells on high dielectric permittivity substrates, the bonding quadrupolar mode can induce a weak Fano resonance in the scattering spectrum of the particle.[39,40]

For a planar metallic nanoparticle or nanostructure deposited on a dielectric substrate, the substrate-induced hybridization of the plasmon modes can be much larger than for a spherical particle, since the plasmon-induced surface charges will be located closer to the dielectric screening charges induced on the surface of the substrate over a large area. In recent studies of the plasmonic properties of silver nanocubes near dielectric substrates,[30,42] evidence of strong coupling between a metallic nanocube and a nearby dielectric substrate was observed. The results show a strong red shift of the nanocube dipolar plasmon and the emergence of a new plasmon resonance with decreasing nanoparticle−substrate separation. This new plasmon mode, appearing on the blue side of the dipolar mode, was found to be remarkably narrow and to exhibit an extraordinary spectral sensitivity to small changes in its dielectric environment.

In this paper, we analyze the plasmon mode interactions of a metallic nanocube on a dielectric substrate. We show that the new plasmon mode observed when the nanocube is close to the substrate is a Fano resonance, originating from the substrate-mediated coupling between two nearly degenerate states: a dark quadrupolar and a bright dipolar nanocube plasmon mode. This picture provides a physically intuitive explanation for the dramatic line shape and the extraordinary LSPR FoM observed for this specific system. More importantly, understanding the underlying origin of the Fano resonance of this system opens a new path for LSPR sensor design that will allow us to optimize the coupling between planar nanostructures and an underlying dielectric substrate for increased sensitivity and response.

The theoretical modeling of a silver nanocube near a dielectric substrate was performed using a commercial software implementation (Comsol Multiphysics) of the finite element method (FEM). By taking the analytical solution of air−dielectric interface (Fresnel formula) as incident excitation, we can model an infinite substrate in the frequency domain.[39] All sharp corners (edges) of the cube in our calculations have been slightly smoothened by spherical (cylindrical) surfaces, to avoid unphysical structural discontinuities. The total scattering cross sections were obtained by integrating the scattered power flux over an enclosed surface outside the cube, while the absorption cross sections were determined by integrating the Ohmic heating within the cube. To describe the silver metal we use experimentally measured silver permittivity data (JC).[43] The glass substrate was modeled using a dielectric permittivity of 2.25. To facilitate the mode analysis, we also used a Drude model (DM) for the silver metal

$$\varepsilon(\omega) = \varepsilon_\infty - \omega_B{}^2/(\omega^2 + i\omega\Gamma)$$

with $\varepsilon_\infty = 4.039$, $\omega_B = 9.172$ eV, and $\Gamma = 0.0207$ eV. This DM neglects the interband transitions above 4 eV but otherwise provides an accurate parametrization of the JC data for Ag.

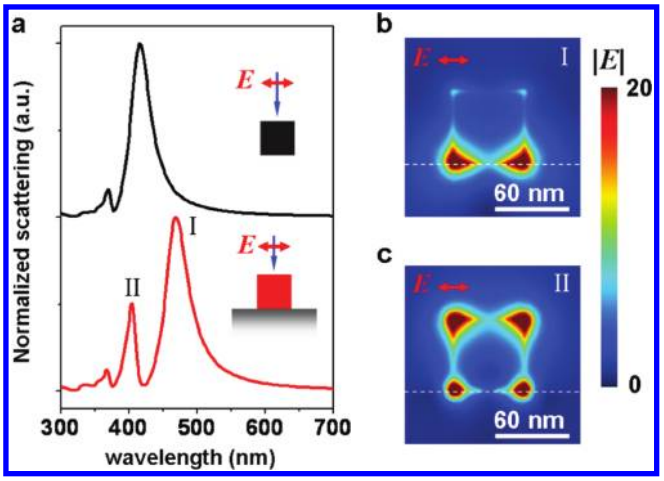

Figure 1. (a) Normalized scattering spectrum of a 60 nm Ag cube in vacuum (black) and on a glass substrate (red), under normal incidence plane wave excitation calculated using FEM and JC. (b, c) Electric field amplitude |**E**| at peak I (469 nm) and peak II (404 nm) in (a), at a plane 1 nm away from the side surface of the cube. The incident light is polarized parallel to the cube edge.

In Figure 1a, the scattering spectra for a 60 nm Ag nanocube in vacuum and on a dielectric substrate are compared. As in the original study of this system by Sherry et al.,[30,42] the dipolar (I) mode is red-shifted and a new mode (II) emerges at 404 nm when the cube contacts the substrate. The line shape of this new mode is highly asymmetric with a steeper slope toward the red than toward the blue. In Figure 1b, the electric field amplitude outside the cube at the scattering peaks I and II, in a plane 1 nm away from the side surface of the cube, is shown. As discussed by Sherry et al.,[30] mode I is oriented toward the substrate while the new mode II is oriented predominantly on the vacuum side. These two modes are the bonding and antibonding hybridized modes resulting from the substrate-mediated interaction of two nearly degenerate dipolar and quadrupolar cube modes. Mode II has an asymmetric line shape because it is a Fano resonance caused by the interference of the dark quadrupolar mode with the continuum of the bright dipolar mode.

To understand the nature of the substrate-mediated hybridization of the cube plasmon modes, we begin by analyzing the plasmonic properties of an individual nanocube in vacuum (Figure 2). An exact mode analysis can only be performed in the electrostatic limit, where there is no radiative damping. We therefore consider a particle size of 3 nm. To also observe higher order cube modes, we use the DM for the silver metal which neglects the damping caused by interband transitions. The results from this electrostatic analysis are qualitatively valid also in the retarded limit and for JC dielectric data. Phase retardation will red shift (dynamic depolarization) and broaden (radiative damping) the plasmon modes but not change their symmetry or spatial distribution.

The primitive (unhybridized) plasmonic modes of a cube in a uniform dielectric medium such as vacuum can be determined analytically.[44−46] Due to its own topology, a cube sustains an infinite number of bright plasmon modes. The six dominant modes shown in Figure 2 account for 93% of the total oscillator strength of the cube.[44,45] This result is quite different from a

metallic sphere, where only three bright dipolar modes exist. The optical absorption spectra in Figure 2a show six bright modes at (i–vi) 376, 342, 330, 310, 301, and 292 nm, respectively. The corresponding charge distributions are shown in Figure 2b. Each mode has a nonzero electric dipole moment and can be excited by an incident plane wave. The dominant mode (i) has its induced charges concentrated on the corners of the cube, with charges of the same sign residing on either side of the cube. This charge distribution is thus characterized by a large electric dipole moment and couples strongly to light.[13] We will refer to this mode (i) as the primitive dipolar (D^0) mode. The dipolar (ii) mode is also present in all spectra discussed here but plays no essential role in the Fano interference.

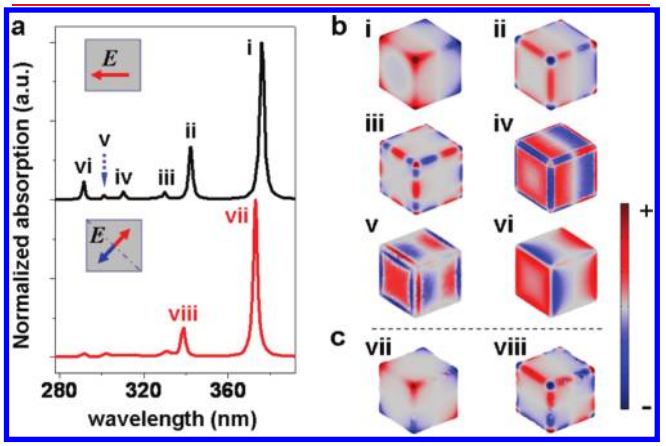

Figure 2. (a) Absorption spectra calculated using FEM and the DM for a 3 nm Ag cube in vacuum, excited by plane wave (black) and dark-mode excitation (red), as indicated in the inset. (b, c) Normalized surface charge distributions of the cube plasmon modes labeled in (a): (b) six bright primitive modes (i–vi); (c) two dark modes (vii, viii).

To identify the dark modes, we used dark-mode excitation,[47] in which an antisymmetric excitation is applied by manually imposing an opposite electric field onto two domains inside the cube, as indicated in the inset of the lower panel of Figure 2a. The corresponding absorption spectrum is shown in the bottom panel of Figure 2a. The pronounced peak (vii) at 373 nm lies very close to the D^0 mode at 376 nm. The charge analysis in Figure 2c shows that this mode has its induced charges concentrated on the corners of the cube like the (i) mode but in a manner such that the overall dipole moment vanishes. The resulting quadrupolar charge distribution cannot couple directly to incident light and the mode is therefore dark. We will refer to this mode (vii) as the primitive quadrupolar (Q^0) mode.

The Q^0 and D^0 modes have almost identical charge distributions on the bottom surface of the cube. Thus when a substrate is present, the induced charges in the substrate will mediate an interaction and the modes will hybridize and form bonding and antibonding states. The near degeneracy of the bright dipolar and dark quadrupolar modes is in strong contrast to the results for a similarly sized solid sphere in vacuum, where the dipolar mode appears at 334 nm and the quadrupolar mode at 318 nm. The small energy difference between the Q^0 and D^0 modes (3 nm) means that the hybridization of these two cube modes will be larger than the hybridization of the dipolar and quadrupolar sphere modes in the presence of the symmetry breaking substrate. It is this near-degeneracy of the dipolar and quadrupolar cube modes, combined with the stronger substrate interaction for a planar structure, that results in the strong Fano resonance in the scattering spectrum of the cube (Figure 1).

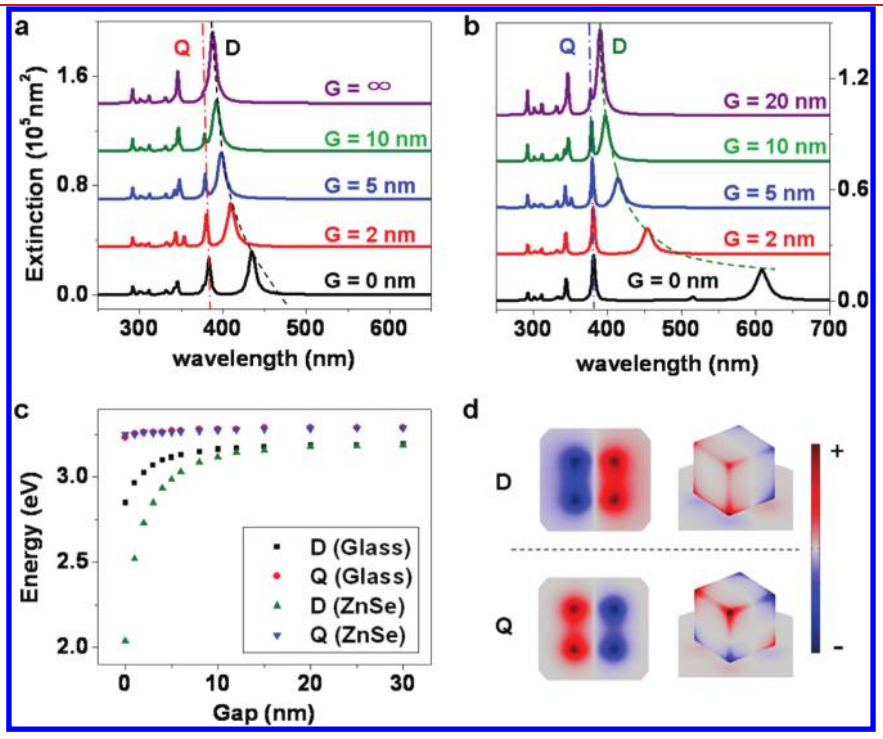

Figure 3. (a, b) Extinction spectra of an individual Ag nanocube (36 nm) on glass (a) and a ZnSe substrate (b) for different cube–substrate separations *G*. (c) Energy of the dipolar (D) and quadrupolar (Q) modes as a function of *G* for glass (black and red) and ZnSe (green and blue). (d) Normalized charge distribution on the substrate surface (left) and the cube surfaces (right) for the D mode at 398 nm and the Q mode at 379 nm for a glass substrate and *G* = 5 nm. The silver is modeled using the DM and the dielectric constants for glass and ZnSe used are 2.25 and 7.5, respectively.

dx.doi.org/10.1021/nl200135r |*Nano Lett.* 2011, 11, 1657–1663

The influence of dielectric substrate on plasmon resonance of a nearby nanoparticle can be rationalized qualitatively using an image charge picture.[39,40] The magnitude of the induced charges depends on the dielectric constant of substrate ε_s, as $(\varepsilon_s - 1)/(\varepsilon_s + 1)$, indicating a stronger interaction for larger ε_s. Panels a and b of Figure 3 show the extinction spectra for a 36 nm Ag cube on glass ($\varepsilon_s = 2.25$) and ZnSe ($\varepsilon_s = 7.5$) substrates for different separations G. When the nanocube is far from the substrate ($G = \infty$), the spectrum is consistent with a cube in the quasi-static regime as shown in Figure 2, except for a very weak shoulder due to the Q^0 mode which is excited due to phase retardation. When the cube approaches the substrate, the D^0 and Q^0 modes begin to interact, and hybridized bonding and antibonding modes are formed. The bonding mode originates from the D^0 mode and weakens and dramatically red shifts with decreasing G. At the same time, the antibonding mode, which originates from the Q^0 mode, gains significant intensity but does not shift appreciably. For simplicity we will refer to the bonding mode as the D mode and the antibonding mode as the Q mode, although both hybridized plasmonic wave functions contain admixtures of D^0 and Q^0 modes. In Figure 3b, a weak mode appearing at 515 nm for $G = 0$ is the result of the strong interaction of the D^0 mode and a higher multipolar cube mode.

The energies of the bonding and antibonding modes for different cube−substrate separations, G, are shown in Figure 3c. The energy shift of the D mode is stronger on the ZnSe substrate because of its larger dielectric constant. The charge distributions on the substrate surface and on the cube surface for the hybridized D and Q modes are shown in Figure 3d for $G = 5$ nm from the glass substrate. The hybridized D mode has most of its charges oriented toward the surface, while the hybridized Q mode is oriented toward the vacuum side. The charge distributions on the substrate reflect the strong coupling between the two modes.

Figure 4 illustrates the substrate-mediated hybridization of the Q^0 and D^0 primitive cube modes. As shown in Figure 4a, a nearby dielectric substrate mediates this interaction and induces hybridization. The energy diagram in Figure 4b (derived from a 36 nm nanocube with $G = \infty$ and $G = 5$ nm in Figure 3a) shows qualitatively how the substrate-mediated interaction results in a bonding D and an antibonding Q mode. It is convenient to separate the substrate effect into two mechanisms: the pure screening effect due to the nearby dielectric and the substrate-mediated interaction of the primitive cube plasmons. The former is the image charge induced by one plasmon mode acting on itself, while the latter refers to the interaction with the other plasmon mode. For weak interaction, the bonding D mode is predominantly D^0 and the antibonding Q is mainly Q^0. As the interaction is increased, the admixture becomes more balanced between D^0 and Q^0. Figure 4c shows the charge distribution for fully hybridized modes, consisting of equal admixtures of D^0 and Q^0. The hybridized states exhibit very different spatial localizations of their plasmon-induced surface charges. The D mode has its charges localized at the cube−substrate interface and the Q mode has its charges localized at the air−cube interface at the top of the cube. The localization of the plasmon-induced field to the air half-space above the cube for the Q mode means that this mode is particularly sensitive to the presence of molecules and contributes significantly to its unusually high LSPR sensitivity.[30]

The hybridization picture presented in Figure 4 provides a qualitative understanding of the spectral changes with decreasing

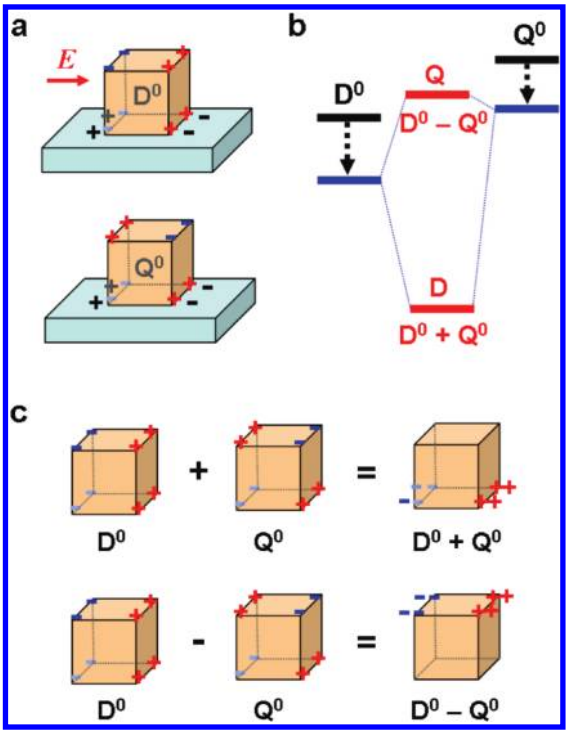

Figure 4. (a) Schematic illustrating the substrate-mediated D^0 and Q^0 interaction. (b) Energy diagram showing the substrate effect: pure dielectric screening effect (dashed black) which causes red shifts of both modes and the substrate-mediated interaction (thin blue line) resulting in hybridized bonding D and antibonding Q modes. (c) Schematic charge distributions of fully hybridized modes $D = D^0 + Q^0$ and $Q = D^0 - Q^0$.

cube−substrate separation shown in panels a and b of Figure 3. For large G, the interaction is weak and only the D mode is visible due to its large dipolar moment. For intermediate G, both the D^0 and Q^0 modes red shift due to the dielectric screening of the substrate. At the same time the splitting of the D and Q modes increases due to the increased substrate-mediated interaction. The strong red shift of the D mode is thus due to both the pure dielectric screening and the increased interaction between the D^0 and Q^0. The very weak shift of the antibonding Q mode is caused by the cancelation of the red shift due to dielectric screening of D^0 and Q^0 and the blue shift due to the increased interaction and hybridization. The increased hybridization with decreasing G transfers dipole moment from the D to the Q modes resulting in a weakening of the spectral intensity of D and a strengthening of the Q modes peak in agreement with the extinction spectra shown in panels a and b of Figure 3.

In Figure 5a we show how the size of the cube influences the Fano interference. The condition for a Fano resonance is a spectral overlap between the narrow subradiant Q mode and the broad superradiant D mode. By changing the dimensions of the structure (scaling with $\eta \times 60$ nm), one can control the radiative damping of the two modes and thus the degree to which they overlap spectrally. For the smallest cube ($\eta = 0.125$) there is no spectral overlap between the Q and D modes and both appear as distinct peaks in the spectrum. As the size of the cube is increased, radiative effects broaden and shift the D mode. The Q mode is only weakly affected by cube size. For η larger than 0.5, the D mode starts overlapping with the Q mode and the characteristic asymmetric Fano resonance appears in the spectrum.

dx.doi.org/10.1021/nl200135r |*Nano Lett.* 2011, 11, 1657–1663

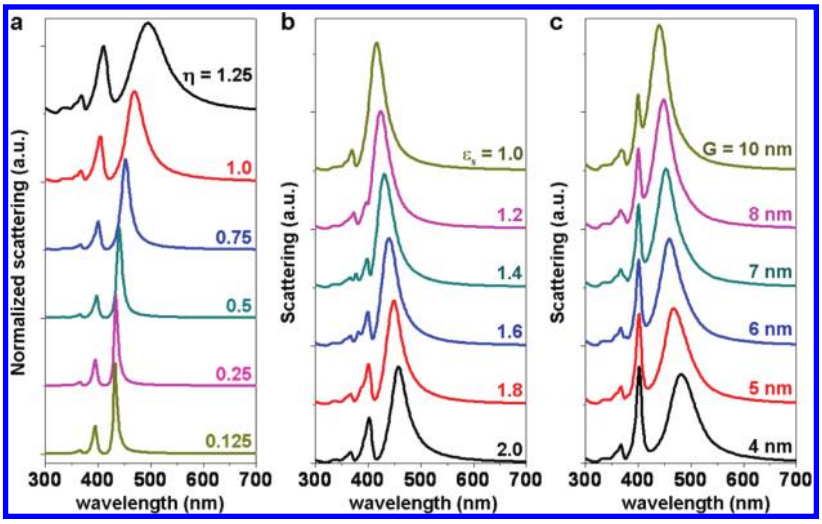

Figure 5. (a) Normalized scattering cross section of a size-scaled silver nanocube in contact with a glass substrate. The dimensions of the cubes are $\eta \times$ 60 nm. (b) Scattering cross section of a 60 nm Ag nanocube on dielectric substrates of different permittivities, ε_s = 2.0, 1.8, 1.6, 1.4, 1.2, and 1.0. (c) Scattering cross section of a 60 nm Ag nanocube on ZnSe substrate for different gaps G = 4, 5, 6, 7, 8, and 10 nm. The silver is modeled using the JC data.

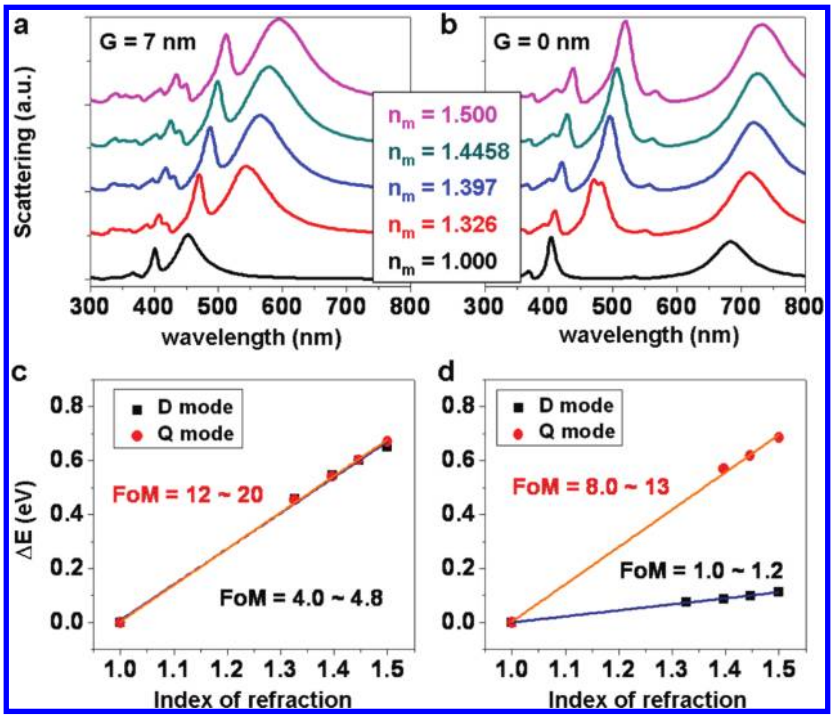

Figure 6. LSPR sensing of the nanocube-on-substrate system. (a, b) Scattering cross section of a 60 nm silver nanocube on ZnSe substrate, in the weak coupling regime with G = 7 nm (a) and in the strong coupling regime with G = 0 nm (b). The index of refraction of the embedding media, n_m, is 1.000 (air, black), 1.326 (methanol, red), 1.397 (butanol, blue), 1.4458 (chloroform, green), and 1.500 (oil, magenta). (c, d) Linear plot of the LSPR shifts of the D (black) and Q (red) mode as a function of refractive index n_m, corresponding to (a) and (b), respectively. The silver is modeled using JC.

The precise conditions for the appearance of the Fano resonance in the nanocube/substrate system are somewhat delicate. For small G, or for substrates of large dielectric permittivity, the splitting between the D and Q modes can become larger than the width of the D resonance. When this happens, there is no Fano interference and both modes appear as well-separated peaks. In Figure 5b, we show how the dielectric permittivity of the substrate influences the scattering spectrum of a 60 nm cube in contact with the substrate (G = 0). For ε_s = 1 (no substrate) no Fano resonance is present. For ε_s = 1.2, mode Q induces a weak Fano resonance at 397 nm. As ε_s is increased, the Fano resonance is enhanced due to a stronger substrate-mediated interaction between the D and Q modes. The sharpest Fano resonance for this case appears at nominally ε_s = 1.6−1.8. For larger ε_s, the red shift of the D mode reduces its spectral overlap with the Q mode and results in less Fano interference, as shown in Figure 3 for ε_s = 2.25 and 7.5, respectively. Figure 5b also shows that for increasing ε_s, the width of the Fano resonance

dx.doi.org/10.1021/nl200135r |*Nano Lett.* 2011, 11, 1657–1663

is increased due to the increasing admixture of the dipolar D^0 component in the hybridized Q mode.

The effect of cube−substrate separation on the nanocube−substrate system is similar to the effect of ε_s. For example, Figure 3b shows clearly a Fano resonance for G = 10 nm, while a much smaller Fano resonance is observable for G = 5 nm because the red shift of the D mode reduces its spectral overlap with the Q mode. In order to illustrate this evolution clearly, in Figure 5c we show the scattering spectra for a 60 nm cube for cube−substrate separations G varying from 4 to 10 nm on a ZnSe substrate. With decreasing G, the red shift of the D mode results in less spectral overlap and a less pronounced Fano resonance. For a given substrate permittivity, the sharpest and most asymmetric Fano resonances will typically appear for a specific G value. For example, for a ZnSe substrate, the optimal separation for a pronounced Fano resonance occurs for G = 7 nm.

To show that Fano interference contributes to large LSPR sensitivity, we compare the LSPR sensing performance of the nanocube-on-substrate system in two coupling regimes: for weak coupling (G = 7 nm) with a pronounced Fano resonance and for strong coupling (G = 0) where the spectral overlap of the Q and D modes is sufficiently reduced so that the Q mode appears more as a distinct peak instead of as a Fano resonance. Figure 6 shows that for both coupling regimes, both the D and Q modes exhibit significant red shifts with increase of the index of refraction of the embedding medium. Linear fit for the peak positions yields a LSPR sensitivity of around 1.3 eV RIU^{-1} for both modes. In the weak coupling regime where a pronounced Fano resonance is present (Figure 6a,c), the effect of an embedding medium (ε_m) is a reduction of the energies of all plasmon modes due to dielectric screening. The embedding medium also decreases the interaction between the modes and thus reduces the blue shift of the Q mode. These combined effects ensure that the conditions for Fano interference remain when embedding media are present. Therefore, the narrow width of the Q mode is preserved, which results in remarkably high FoMs ranging from 12 (fwhm calculated from ε_m = 1.5) to 20 (fwhm calculated from ε_m = 1.0). For the strong coupling regime (Figure 6b,d), the increased width of the Q resonance reduces the FoMs to 8−13. For both coupling regimes, the FoM of the bright D mode is significantly smaller than that for the Q mode.

The present analysis has been concerned exclusively with cubes, where all sides have the same dimensions. The strong interaction and hybridization of the primitive cube modes through the underlying substrate is due to the unique geometry of a perfect cube, where the parent D^0 and Q^0 modes have very similar energies. The conditions for a strong Fano resonance can be much easier satisfied for a rectangular block with sides of different lengths. This extra degree of structural freedom allows the independent tuning of both the D^0 and Q^0 modes and their interaction through the substrate. This is likely to be an important consideration in the analysis and assignment of the plasmon modes of planar nanostructures patterned and deposited by clean-room fabrication methods. A more detailed investigation of the geometrical tunability of the nanoblock/substrate system and its relevance for LSPR sensing will be presented in a future publication.

In conclusion, using the plasmon hybridization concept we have theoretically examined the plasmonic properties of an Ag nanocube on dielectric substrate. We show that the distinct double peak plasmonic structure observed in the scattering spectrum is due to Fano interference, caused by the substrate-mediated interaction of a dark quadrupolar cube mode with a bright dipolar cube mode. This insight provides a path for optimizing an easily manufacturable geometry, planar nanostructures on dielectric substrates with controlled separations, as plasmonic Fano-resonant LSPR sensors with high-performance sensitivities.

AUTHOR INFORMATION

Corresponding Author
*E-mail: nordland@rice.edu.

ACKNOWLEDGMENT

The authors thank Mr. Heidar Sobhani for valuable discussions. P.N. and N.J.H. acknowledge support from The Robert A. Welch Foundation (C-1220 and C-1222); the Center for Solar Photophysics, an Energy Frontier Research Center funded by U. S. Department of Energy; and the NSF under Grant CNS-0821727 and the Office of Naval Research (N00244-09-1-0067). H.X. acknowledges NSFC Grant No. 10874233, MOST Grants (Nos. 2007CB936800 and 2009CB930700), and the "Knowledge Innovation Project" of CAS under grant KJCX2-EW-W04.

REFERENCES

(1) Sau, T. K.; Rogach, A. L.; Jäckel, F.; Klar, T. A.; Feldmann, J. *Adv. Mater.* **2010**, *22* (16), 1805–1825.
(2) Lin, S. X.; Wong, C. Y.; Pun, E. Y. B.; Song, F. *Nanotechnology* **2010**, *21* (5), 055203.
(3) Rycenga, M.; Camargo, P. H. C.; Li, W. Y.; Moran, C. H.; Xia, Y. N. *J. Phys. Chem. Lett.* **2010**, *1* (4), 696–703.
(4) Li, Z. Y.; Xia, Y. N. *Nano Lett.* **2010**, *10* (1), 243–249.
(5) Teo, S. L.; Lin, V. K.; Marty, R.; Large, N.; Llado, E. A.; Arbouet, A.; Girard, C.; Aizpurua, J.; Tripathy, S.; Mlayah, A. *Opt. Express* **2010**, *18* (21), 22271–22282.
(6) Aubry, A.; Lei, D. Y.; Fernández-Domínguez, A. I.; Sonnefraud, Y.; Maier, S. A.; Pendry, J. B. *Nano Lett.* **2010**, *10* (7), 2574–2579.
(7) Kawata, S.; Inouye, Y.; Verma, P. *Nat. Photonics* **2009**, *3* (7), 388–394.
(8) Huang, J. S.; Kern, J.; Geisler, P.; Weinmann, P.; Kamp, M.; Forchel, A.; Biagioni, P.; Hecht, B. *Nano Lett.* **2010**, *10* (6), 2105–2110.
(9) Yang, S. C.; Kobori, H.; He, C. L.; Lin, M. H.; Chen, H. Y.; Li, C. C.; Kanehara, M.; Teranishi, T.; Gwo, S. *Nano Lett.* **2010**, *10* (2), 632–637.
(10) Golden, M. S.; Bjonnes, A. C.; Georgiadis, R. M. *J. Phys. Chem. C* **2010**, *114* (19), 8837–8843.
(11) Rang, M.; Jones, A. C.; Zhou, F.; Li, Z. Y.; Wiley, B. J.; Xia, Y. N.; Raschke, M. B. *Nano Lett.* **2008**, *8* (10), 3357–3363.
(12) Palomba, S.; Novotny, L. *Nano Lett.* **2009**, *9* (11), 3801–3804.
(13) Kim, D. S.; Heo, J.; Ahn, S. H.; Han, S. W.; Yun, W. S.; Kim, Z. H. *Nano Lett.* **2009**, *9* (10), 3619–3625.
(14) Woolf, D.; Loncar, M.; Capasso, F. *Opt. Express* **2009**, *17* (22), 19996–20011.
(15) Kang, M.; Park, J.; Lee, I. M.; Lee, B. *Opt. Express* **2009**, *17* (2), 676–687.
(16) Wang, H.; Brandl, D. W.; Nordlander, P.; Halas, N. J. *Acc. Chem. Res.* **2007**, *40* (1), 53–62.
(17) Liu, H.; Li, T.; Wang, S. M.; Zhu, S. N. *Front. Phys. China* **2010**, *5* (3), 277–290.
(18) Davis, T. J.; Gómez, D. E.; Vernon, K. C. *Nano Lett.* **2010**, *10* (7), 2618–2625.
(19) Hentschel, M.; Saliba, M.; Vogelgesang, R.; Giessen, H.; Alivisatos, A. P.; Liu, N. *Nano Lett.* **2010**, *10* (7), 2721–2726.
(20) Choi, C. L.; Alivisatos, A. P. *Annu. Rev. Phys. Chem.* **2010**, *61*, 369–389.

(21) Ye, J.; Van Dorpe, P.; Lagae, L.; Maes, G.; Borghs, G. *Nanotechnology* **2009**, *20* (46), No. 465203.
(22) Luk'yanchuk, B.; Zheludev, N. I.; Maier, S. A.; Halas, N. J.; Nordlander, P.; Giessen, H.; Chong, C. T. *Nat. Mater.* **2010**, *9* (9), 707–715.
(23) Miroshnichenko, A. E.; Flach, S.; Kivshar, Y. S. *Rev. Mod. Phys.* **2010**, *82* (3), 2257–2298.
(24) Liu, N.; Liu, H.; Zhu, S. N.; Giessen, H. *Nat. Photonics* **2009**, *3* (3), 157–162.
(25) Pakizeh, T.; Langhammer, C.; Zorić, I.; Apell, P.; Käll, M. *Nano Lett.* **2009**, *9* (2), 882–886.
(26) Pakizeh, T.; Käll, M. *Nano Lett.* **2009**, *9* (6), 2343–2349.
(27) Hao, F.; Sonnefraud, Y.; Van Dorpe, P.; Maier, S. A.; Halas, N. J.; Nordlander, P. *Nano Lett.* **2008**, *8* (11), 3983–3988.
(28) Liu, N.; Weiss, T.; Mesch, M.; Langguth, L.; Eigenthaler, U.; Hirscher, M.; Sönnichsen, C.; Giessen, H. *Nano Lett.* **2010**, *10* (4), 1103–1107.
(29) Lassiter, J. B.; Sobhani, H.; Fan, J. A.; Kundu, J.; Capasso, F.; Nordlander, P.; Halas, N. J. *Nano Lett.* **2010**, *10* (8), 3184–3189.
(30) Sherry, L. J.; Chang, S. H.; Schatz, G. C.; Van Duyne, R. P.; Wiley, B. J.; Xia, Y. N. *Nano Lett.* **2005**, *5* (10), 2034–2038.
(31) Gómez, D. E.; Vernon, K. C.; Davis, T. J. *Phys. Rev. B* **2010**, *81* (7), No. 075414.
(32) Neubrech, F.; Kolb, T.; Lovrincic, R.; Fahsold, G.; Pucci, A.; Aizpurua, J.; Cornelius, T. W.; Toimil-Molares, M. E.; Neumann, R.; Karim, S. *Appl. Phys. Lett.* **2006**, *89* (25), No. 253104.
(33) Hu, Y.; Noelck, S. J.; Drezek, R. A. *ACS Nano* **2010**, *4* (3), 1521–1528.
(34) Mukherjee, S.; Sobhani, H.; Lassiter, J. B.; Bardhan, R.; Nordlander, P.; Halas, N. J. *Nano Lett.* **2010**, *10* (7), 2694–2701.
(35) Sheikholeslami, S.; Jun, Y. W.; Jain, P. K.; Alivisatos, A. P. *Nano Lett.* **2010**, *10* (7), 2655–2660.
(36) Brown, L. V.; Sobhani, H.; Lassiter, J. B.; Nordlander, P.; Halas, N. J. *ACS Nano* **2010**, *4* (2), 819–832.
(37) Aydin, K.; Pryce, I. M.; Atwater, H. A. *Opt. Express* **2010**, *18* (13), 13407–13417.
(38) Yang, Z. J.; Zhang, Z. S.; Zhang, W.; Hao, Z. H.; Wang, Q. Q. *Appl. Phys. Lett.* **2010**, *96* (13), No. 131113.
(39) Knight, M. W.; Wu, Y. P.; Lassiter, J. B.; Nordlander, P.; Halas, N. J. *Nano Lett.* **2009**, *9* (5), 2188–2192.
(40) Wu, Y. P.; Nordlander, P. *J. Phys. Chem. C* **2010**, *114* (16), 7302–7307.
(41) Vernon, K. C.; Funston, A. M.; Novo, C.; Gómez, D. E.; Mulvaney, P.; Davis, T. J. *Nano Lett.* **2010**, *10* (6), 2080–2086.
(42) McMahon, J. A.; Wang, Y. M.; Sherry, L. J.; Van Duyne, R. P.; Marks, L. D.; Gray, S. K.; Schatz, G. C. *J. Phys. Chem. C* **2009**, *113* (7), 2731–2735.
(43) Johnson, P. B.; Christy, R. W. *Phys. Rev. B* **1972**, *6* (12), 4370–4379.
(44) Fuchs, R. *Phys. Rev. B* **1975**, *11* (4), 1732–1739.
(45) Ruppin, R. *Z. Phys. D* **1996**, *36* (1), 69–71.
(46) Klimov, V. V.; I., Y. N.; Kosevich., Yu A. *Phys.-Usp.* **2008**, *51* (8), 839–859.
(47) Koh, A. L.; Bao, K.; Khan, I.; Smith, W. E.; Kothleitner, G.; Nordlander, P.; Maier, S. A.; McComb, D. W. *ACS Nano* **2009**, *3* (10), 3015–3022.